

Nanoscale

Accepted Manuscript



This is an *Accepted Manuscript*, which has been through the Royal Society of Chemistry peer review process and has been accepted for publication.

Accepted Manuscripts are published online shortly after acceptance, before technical editing, formatting and proof reading. Using this free service, authors can make their results available to the community, in citable form, before we publish the edited article. We will replace this *Accepted Manuscript* with the edited and formatted *Advance Article* as soon as it is available.

You can find more information about *Accepted Manuscripts* in the [Information for Authors](#).

Please note that technical editing may introduce minor changes to the text and/or graphics, which may alter content. The journal's standard [Terms & Conditions](#) and the [Ethical guidelines](#) still apply. In no event shall the Royal Society of Chemistry be held responsible for any errors or omissions in this *Accepted Manuscript* or any consequences arising from the use of any information it contains.

**Band Structure Engineering of Monolayer MoS₂ by Surface Ligand
Functionalization for Enhanced Photoelectrochemical Hydrogen production
Activity**

Jing Pan^{1,2}, Zilu Wang¹, Qian Chen¹, Jingguo Hu², Jinlan Wang^{1*}

¹Department of Physics & Key Laboratory of MEMS of Ministry of Education, Southeast
University, Nanjing, 211189, China

²College of Physics Science and Technology, Yangzhou University, Yangzhou, 225002, China

Abstract:

To achieve photoelectrochemical (PEC) activity of MoS₂ for hydrogen production through water-splitting, the band edges of MoS₂ should match with the hydrogen and oxygen production levels. Our first-principles calculations show that the band edges of monolayer MoS₂ can be effectively tuned by surface ligand functionalization, resulting from the intrinsic dipole of ligand itself and the induced dipole at the interface of ligand/MoS₂. We further explore the influence of ligand coverage, ligand functionalization and the substrate on the band structure of MoS₂. The hybrid C₆H₅CH₂NH₂/MoS₂/graphene structures may be compelling candidate as they satisfy stringent requirements of PEC water-splitting.

* Email: jlwang@seu.edu.cn

1. Introduction

Photoelectrochemical (PEC) water-splitting to generate hydrogen has attracted extensive attentions as a potential means of renewable energy production.¹⁻⁵ Over the past decades, many semiconductors have been used as photocatalyst although the efficiency of PEC water-splitting is still low and far from practical application. The major obstacle to progress in this field is the lack of ideal semiconductor photocatalyst that satisfy the requirements⁶ of 1) appropriate band gap (1.6 – 2.2 eV) for efficient visible light absorption; 2) high carrier mobility; 3) suitable band edge positions that straddle the water redox potentials; 4) chemical stability to corrosion and photocorrosion in aqueous environments. Therefore, searching and engineering efficient and stable semiconductor photocatalyst is still a hot research topic.

Recently, molybdenum disulfide (MoS_2) has been extensively investigated.⁷⁻¹² It is a layered hexagonal structure with weak van der Waals interaction between individual sandwiched S-Mo-S layers.^{13,14} Bulk MoS_2 has an indirect band gap of 1.2 eV.¹⁵ Monolayer MoS_2 (ML- MoS_2) has a direct band gap of ~ 1.8 eV,^{16,17} which is ideal for solar energy absorption. It was reported that the mobility of MoS_2 can even be as large as $200 \text{ cm}^2\text{V}^{-1}\text{s}^{-1}$ at room temperature⁸ although much lower values were obtained in other experiments^{18,19} which might originate from the existence of short-range surface defects.¹⁹ Moreover, ML- MoS_2 exhibits high electrocatalytic activity and stability for the hydrogen evolution reaction (HER) in acidic environment.²⁰⁻²² These advantages make ML- MoS_2 potential candidate for PEC water-splitting. Nevertheless, the conduction band minimum (CBM) of ML- MoS_2 is below the hydrogen redox potential of water, excited electrons cannot reduce hydrogen through photoelectrocatalytic HER, which limits its application in PEC water-splitting.^{23,24}

Experimental and theoretical explorations have shown that surface functionalization with organic molecules or “surface ligands” have great influences on the electronic and optical properties of nanostructures.²⁵⁻²⁹ Specifically, surface ligand functionalization has been predicted to effectively tailor the semiconductor band edge energies (e.g., CdSe and Si) from first-principles calculations,^{27,29} and confirmed later in experiment.²⁸ In this article, we investigate the possibility of ML-MoS₂ for PEC water-splitting by surface ligand functionalization. Our first-principle calculations show that band edge positions can be effectively engineered in a broad range by either choosing different ligand groups or functionalizing ligands. The influences of ligand coverage and the substrate are further discussed. The band shifts mainly arise from the intrinsic dipole of ligands and the induced dipole at ligand/MoS₂ interface, and hybrid C₆H₅CH₂NH₂/MoS₂/graphene structures may be good candidate for PEC water-splitting.

2. Computational Model and Details

All calculations were performed using density functional theory (DFT) with the general gradient approximation of the Perdew-Burke-Eznerhof³⁰ including van der Waal (vdW) corrections,³¹ as implemented in the Vienna ab initio simulation package.³² The frozen-core projector-augmented-wave³³ method was employed to describe the electron-ion interaction and the cutoff energy for the plane-wave basis set was 400 eV. The Monkhorst-Pack k -point was used for integration over the first Brillouin zone. $7 \times 7 \times 1$ and $11 \times 11 \times 1$ k -point meshes were adopted for geometry optimization and electronic structure calculations, respectively. The dipole correction was applied to avoid spurious electrostatic interactions between the

periodic slabs.³⁴⁻³⁶ All atomic positions and lattice constants were optimized until the Hellmann-Feynman forces acting on each atom and the total energy change were less than 0.01 eV/Å and 1.0×10^{-4} eV, respectively. The calculated lattice constants ($a = b = 3.17$ Å) of bulk MoS₂ are in fair agreement with the experimental values ($a = b = 3.16$ Å).³⁷

ML-MoS₂ was built by cleaving from the (0001) surface of bulk MoS₂ and incorporating a vacuum larger than 15 Å to ensure decoupling between neighboring slabs. As shown in Fig. 1, a 2×2 supercell was used to select suitable ligands for surface functionalization. The functionalization groups include mono-atomic group (*e.g.* F), oxygen-containing group (*e.g.* O₂, H₂O, COOH) and benzene-containing group (*e.g.* benzonitrile (C₆H₅CN) and benzylamine (C₆H₅CH₂NH₂)), which have different dipole moments of 0, 1.859, 1.960, 4.702 and 1.407 D for O₂, H₂O, COOH, C₆H₅CN and C₆H₅CH₂NH₂, respectively. To explore the influence of ligand coverage on band edge positions, we considered ligand coverage with 25%, 18.75%, 12.5%, 11.1%, 6.25% and 4% by adsorbing the ligands on a 2×2, 3×3, 4×4 and 5×5 MoS₂ supercell, respectively. Furthermore, hybrid MoS₂/graphene heterostructure was built to investigate the effect of the substrate, where a 4×4 MoS₂ supercell was placed on a 5×5 graphene supercell with the mismatch of 1.38%.

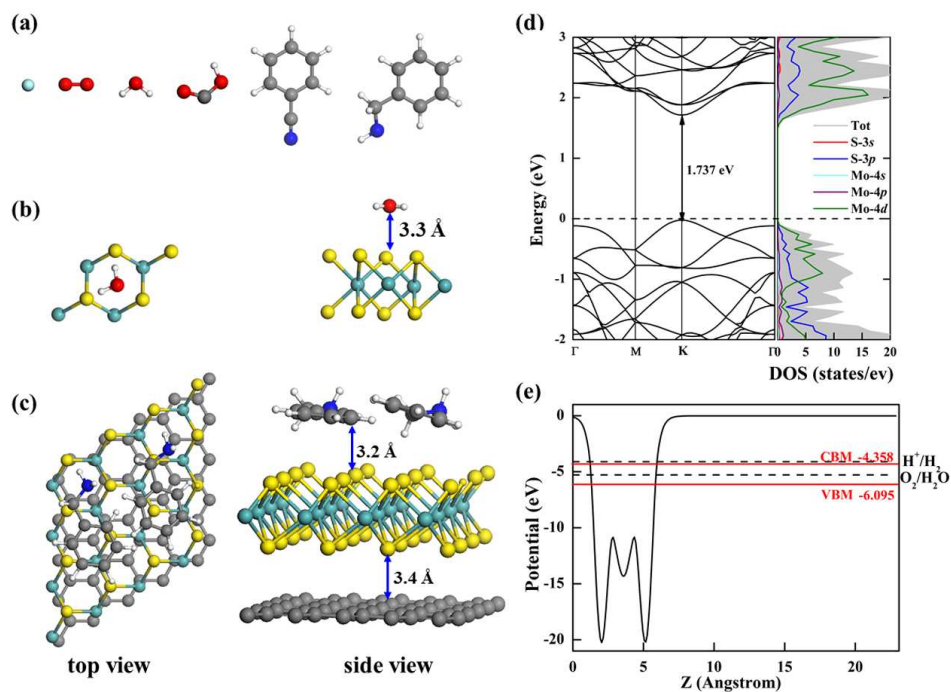


Fig. 1 (a) Atomic structure of isolated F, O₂, COOH, H₂O, C₆H₅CN and C₆H₅CH₂NH₂. Top and side views of (b) H₂O adsorption on a 2×2 ML-MoS₂ and (c) C₆H₅CN adsorption on a MoS₂/graphene hybrid system, where MoS₂ is a 4×4 supercell and graphene is a 5×5 supercell. (d) Band structure and atom-partial DOS of ML-MoS₂. (e) Average electrostatic potential of ML-MoS₂ (black solid line), where the vacuum level is set to be zero. The red solid lines denote the calculated CBM and VBM, and the black dash lines refer to the water redox potential positions at pH = 7, respectively.

3. Results and Discussion

As shown in Fig. 1(d) and (e), the calculated band gap of ML-MoS₂ is 1.737eV. Both VBM and CBM are comprised mainly of Mo 4*d* and slightly of S 3*p* states, and VBM is below the water oxidation level whereas CBM locates below the hydrogen redox potential. The calculation details of the average electrostatic potential and band edge positions of ML-MoS₂ are given in Supporting Information.³⁸ These results are all in good agreement with the experimental values.^{16, 24}

3.1 Choosing the suitable surface functionalization ligand

We first consider the surface functionalization of ML-MoS₂ by various ligand groups including F, O₂, H₂O, COOH, C₆H₅CN and C₆H₅CH₂NH₂, to determine the most suitable surface functionalization ligand for PEC water-splitting. Three adsorption sites, including the top site of S (T_S) and Mo atom (T_M), and the hollow site of the hexagonal lattice (H site), were considered. The initial ligand orientations were set to be perpendicular or parallel to the surface and the optimized most stable structures are presented in Fig. S1 in the Supporting Information.³⁸ The binding energy of the ligand to MoS₂, defined as $E_b = E_{\text{MoS}_2} + E_{\text{ligand}} - E_{\text{tot}}$ (E_{MoS_2} , E_{ligand} and E_{tot} are the energies of isolated ML-MoS₂, ligand and hybrid ligand/MoS₂ structure), varies in the range of ~ 0.1-2.0 eV. The F atom is found to strongly adsorb on MoS₂ with a large binding energy of about 2.0 eV and a covalent F-S bond is formed with a bond length of 1.74 Å. For O₂, H₂O, COOH, C₆H₅CN and C₆H₅CH₂NH₂ functionalized MoS₂, no chemical bond is formed between the ligand and the surface and the distance between them is about 3 Å, suggesting physisorption between these ligands and MoS₂. For O₂ and H₂O adsorption, the binding energy is small (0.148 and 0.185 eV, respectively). For C₆H₅CN and C₆H₅CH₂NH₂, it rises up to 0.541 and 0.731 eV, respectively. The increase of the binding strength is attributed to the large size and the molecular polarity of C₆H₅CN and C₆H₅CH₂NH₂. Actually, relatively large binding energies were also obtained in literature. For example, the binding energy of benzene and naphthalene adsorbing on MoS₂ is 0.47 and 0.70 eV³⁹.

The band structures and density of states (DOS) of functionalized MoS₂ are displayed in Fig. 2. Except for the case of F functionalization, the other surface ligands do not bring much change to the band gaps, varying from ~ 1.74 to 1.75 eV, while they greatly alter the band

edge positions of MoS₂. The chemical adsorption of F atom turns the semiconductor MoS₂ into a metal accompanying with the appearance of impurity bands which are from the hybridization of F-2*p* orbitals, S-3*p* and Mo-4*d* across the Fermi level. Though O₂ functionalized MoS₂ maintains the properties of the semiconductor, the isolated LUMO state of O₂ locates deeply within the band gap, which can easily act as the carrier recombination center and reduce the photogenerated current.⁴⁰ Similar to O₂ functionalization, both the HOMO and LUMO states locate deeply within the band gap for COOH functionalization. Differently, the HOMO state of C₆H₅CH₂NH₂ is close to the VBM of MoS₂ and hybrids with the host states of MoS₂ (Mo-4*d* and S-3*p* states), forming shallow impurity levels, which are less likely to form recombination centers. Such shallow impurity levels are actually beneficial for optical absorption⁴⁰ because the electrons in the VB can be easily excited to them and subsequently to CB. For H₂O and C₆H₅CN functionalized MoS₂, both the HOMO and LUMO of molecules are presented deeply in the VB and CB of MoS₂ and hybrid with the host states, which should have negligible impact on the efficiency of optical absorption of MoS₂. Therefore, we can expect that H₂O, C₆H₅CN and C₆H₅CH₂NH₂ functionalized ML-MoS₂ may have high efficiency in photocatalysis because of their ideal band gaps for visible light absorption and the absence of electron-hole recombination center.

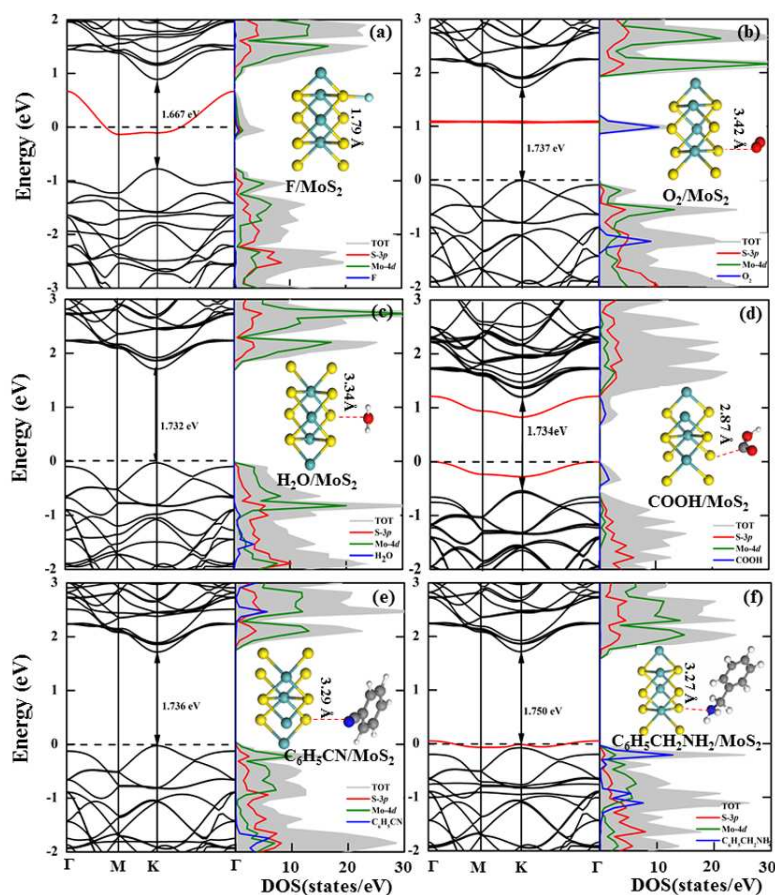


Fig. 2 Band structure and DOS of ML-MoS₂ surface functionalized by (a) F, (b) O₂, (c) H₂O, (d) COOH, (i) C₆H₅CN and (j) C₆H₅CH₂NH₂.

To evaluate whether these hybrid MoS₂ structures are proper for PEC water-splitting, we further calculate band edge positions of pure, H₂O, C₆H₅CN and C₆H₅CH₂NH₂ functionalized MoS₂ and compare with water redox potentials in Fig. 3. For H₂O/MoS₂, the band edge positions overall down-shift by ~ 0.117 eV in comparison with pure MoS₂ and the CBM position is lower than the hydrogen production potential, suggesting that it is not suitable for PEC water-splitting. For C₆H₅CN/MoS₂ and C₆H₅CH₂NH₂/MoS₂, the band edge positions up-shift by ~ 1.534 and ~ 0.774 eV, respectively. C₆H₅CH₂NH₂/MoS₂ well matches with the redox potentials of water. For the case of C₆H₅CN/MoS₂, the band edges up-shift so large that the VBM is above the potential of water oxidation. Nevertheless, the shift may be tuned to the ideal value by controlling surface ligand coverage. Therefore, C₆H₅CN and C₆H₅CH₂NH₂ are

chosen as surface functionalization ligands for MoS₂ based PEC water-splitting.

Fig. 3 displays the charge density difference of these ligand functionalized MoS₂ hybrid systems, which is defined as $\Delta\rho = \rho(\text{ligand/MoS}_2) - \rho(\text{MoS}_2) - \rho(\text{ligand})$, where $\rho(\text{ligand/MoS}_2)$, $\rho(\text{MoS}_2)$ and $\rho(\text{ligand})$ are the electronic charge density of the hybrid systems, isolated MoS₂ surface and ligand in frozen geometry, respectively. As clearly seen from the figure, no overlapping is observed between the ligands and MoS₂, reflecting the weak interaction between ligand and MoS₂. Interestingly, although the charge transfer between ligands and the surface is very small, we observe charge transfer from MoS₂ to H₂O, and from C₆H₅CN and C₆H₅CH₂NH₂ to MoS₂. These are also reflected by Bader charge analysis⁴¹ that there are $\sim 0.006 e$ charge transferred from MoS₂ to H₂O, $0.005 e$ and $0.013 e$ from C₆H₅CN and C₆H₅CH₂NH₂ to MoS₂, respectively.

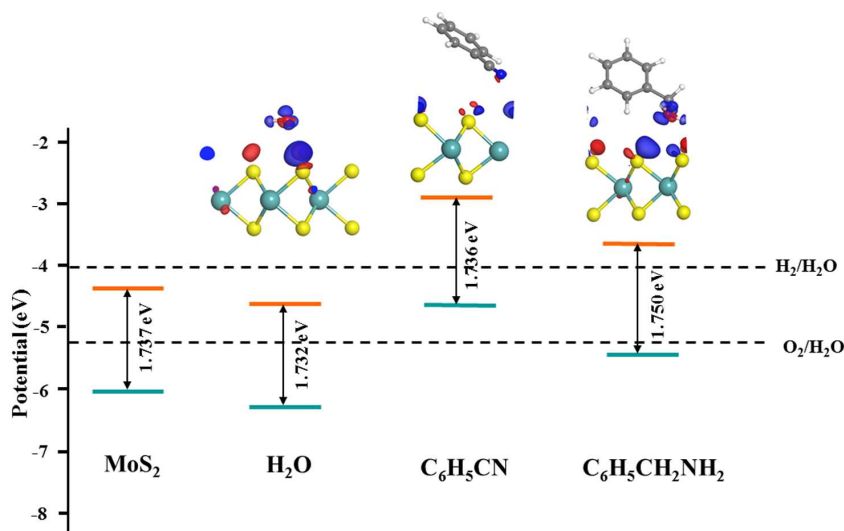


Fig. 3 Calculated band edge positions of MoS₂, H₂O, C₆H₅CN and C₆H₅CH₂NH₂ functionalized MoS₂ in comparison with water redox potentials and charge density difference of these hybrid systems, with red and blue colors representing charge accumulation and charge depletion, respectively. The isovalue is $0.004 e/\text{\AA}^3$.

The shift of band edges can be interpreted in light of charge-induced dipole interaction including the intrinsic dipole of the ligand, μ_{ligand} , and the induced dipole at ligand/MoS₂

interface, μ_{ind} , associated with the geometry distortion and charge rearrangement, which is also observed in the ligand functionalized CdSe surface.²⁷ In this model, the energy shift of an ejected electron or hole with respect to the vacuum level, that is the work function change ΔW_{\perp} , arising from the dipole perpendicular to the surface, can be expressed as $\Delta W_{\perp} = \mu_{\perp} / A \epsilon_0$, where A is the surface area per ligand, ϵ_0 is the dielectric constant of the vacuum, and μ_{\perp} is the total dipole of the perpendicular component of the intrinsic dipole of the free-standing ligand layer without substrate, and the induced dipole at interface, *i.e.*, $\mu_{\perp} = \mu_{\text{ligand}, \perp} + \mu_{\text{ind}, \perp}$. This definition automatically incorporates the effect of the depolarizing electric field caused by the ligand dipoles surrounded, which is usually introduced as an effective dielectric constant in the ligand layer.³⁴⁻³⁶ The work function change will lead to the band edge shift on the opposite direction, *i.e.*, $\Delta V_{\perp} = -\Delta W_{\perp}$. As shown in Table I, taking C₆H₅CN/MoS₂ as an example, the total dipole density is $\mu_{\perp}/A = -4.071 \text{ D/nm}^2$, in which the dipole density of the ligand layer $\mu_{\text{ligand}, \perp}/A$ is -3.803 D/nm^2 and the induced dipole density at interface $\mu_{\text{ind}, \perp}/A$ is -0.269 D/nm^2 . The induced interface dipole density is very small because of the relatively weak interaction between the ligand and surface. Therefore, the resultant work function change ΔW_{\perp} (-1.534 eV) and the band edge up-shifts (1.534 eV) are primarily from the intrinsic dipole moment of the ligand, which is in agreement with the energy shift calculated via the average electrostatic potential, (also see Fig. S2 in Supporting Information).³⁸

Table I. Band gap E_g (in eV), VBM and CBM positions E_{VBM} and E_{CBM} (in eV) of ligand functionalized MoS₂, the work function change ΔW_{\perp} (in eV) of functionalized MoS₂ relative to pure MoS₂, total dipole density μ_{\perp}/A (in D/nm^2) of hybrid ligand/MoS₂, intrinsic dipole density $\mu_{\text{ligand}, \perp}/A$ (in D/nm^2) of ligand and induced dipole density $\mu_{\text{ind}, \perp}/A$ (in D/nm^2) at ligand/MoS₂ interface perpendicular to the surface.

System	E_g	E_{VBM}	E_{CBM}	ΔW_{\perp}	μ_{\perp}/A	$\mu_{\text{ligand}, \perp}/A$	$\mu_{\text{ind}, \perp}/A$
Pure	1.737	-6.095	-4.358	-	-	-	-
H ₂ O	1.732	-6.212	-4.480	0.117	0.310	0.437	-0.127

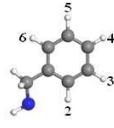
C_6H_5CN	1.736	-4.560	-2.824	-1.534	-4.071	-3.803	-0.269
$C_6H_5CH_2NH_2$	1.750	-5.321	-3.571	-0.774	-2.054	-1.537	-0.517

3.2 F substitutionally doped ligand functionalized MoS_2

Since the intrinsic ligand dipole and the induced interface dipole have great influence on the band edge positions, we can further tailor the band structure by doping the ligand and thereby altering the interface dipole of ligand/ MoS_2 . C_6H_5CN and $C_6H_5CH_2NH_2$ are chosen to be doped by substituting an H atom with an F atom at different sites of the benzene ring. Fig. 4 shows the band gap and band edge positions of F doped C_6H_5CN and $C_6H_5CH_2NH_2$ functionalized MoS_2 . Comparing to undoped situations, the positions of band edge change greatly. As presented in Table II, though the band gap of functionalized MoS_2 does not alter much, the band edges can be efficiently tuned in a broad range. The work function changes are about -1.861, -1.411 and -0.946 eV when F substitutes H at site 2, 3 and 4 for C_6H_5CN functionalized MoS_2 , respectively, leading to the significant up-shift of the band edge. For F doped $C_6H_5CH_2NH_2$ functionalized MoS_2 , the work function changes range from -0.98 to 0.25 eV, which results from the functionalization induced intrinsic dipole moment $\mu_{ligand,\perp}$ (from -2.184 to 1.187 D/nm²) and the induced dipole moment $\mu_{ind,\perp}$ (from -0.697 to -0.399 D/nm²). For F doped $C_6H_5CH_2NH_2/MoS_2$ at site 5, the large positive intrinsic dipole moment (1.187 D/nm²), prevails the negative induced dipole moment (-0.531 D/nm²), leading to the down-shift of the band edge (~ 0.247 eV). While for F doped $C_6H_5CH_2NH_2$ at site 3, the density of intrinsic and induced dipole moment increases to -1.899 and -0.697 D/nm², respectively, which gives rise to the up-shift of the maximum band edge by 0.979 eV. This is because the substitution of H with F at different sites changes the favored orientation of the

ligand on the surface, which produces extra intrinsic dipole moment along the surface perpendicular direction and alters the induced interface dipole moment accordingly.

Table II. Site of F doped ligand for C_6H_5CN and $C_6H_5CH_2NH_2$, band gap E_g (in eV), VBM and CBM positions E_{VBM} and E_{CBM} (in eV) of ligand functionalized MoS_2 , the work function change ΔW_{\perp} (in eV) of functionalized MoS_2 relative to pure MoS_2 , total dipole density μ_{\perp}/A (in D/nm^2) of the ligand/ MoS_2 hybrid system, intrinsic dipole density $\mu_{ligand,\perp}/A$ (in D/nm^2) of ligands and induced dipole density $\mu_{int,\perp}/A$ (in D/nm^2) at ligand/ MoS_2 interface perpendicular to the surface.

System	site	E_g	E_{VBM}	E_{CBM}	ΔW_{\perp}	μ_{\perp}/A	$\mu_{ligand,\perp}/A$	$\mu_{int,\perp}/A$
MoS_2	-	1.737	-6.095	-4.358	-	-	-	-
	ligand	1.736	-4.560	-2.824	-1.534	-4.071	-3.803	-0.269
	F_2	1.735	-4.234	-2.499	-1.861	-4.938	-4.655	-0.283
	F_3	1.736	-4.684	-2.947	-1.411	-3.743	-3.304	-0.439
	F_4	1.735	-5.149	-3.414	-0.946	-2.509	-2.210	-0.299
	ligand	1.750	-5.321	-3.571	-0.774	-2.054	-1.537	-0.517
	F_2	1.774	-5.122	-3.348	-0.973	-2.583	-2.184	-0.399
	F_3	1.749	-5.116	-3.367	-0.979	-2.596	-1.899	-0.697
	F_4	1.755	-5.770	-4.015	-0.325	-0.863	-0.321	-0.542
	F_5	1.882	-6.342	-4.460	0.247	0.656	1.187	-0.531
	F_6	1.788	-5.600	-3.812	-0.495	-1.314	-0.891	-0.423

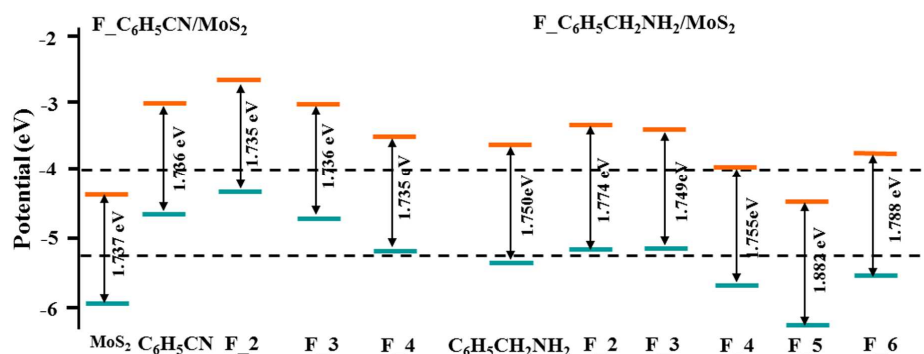


Fig. 4 Calculated band edge positions of pure, and F functionalized C_6H_5CN and $C_6H_5CH_2NH_2$ functionalized MoS_2 in comparison with water redox potentials.

3.3 The effect of ligand coverage on the band structure

We next explore the influence of ligand coverage on the band structure of MoS_2 . Fig. 5 shows the binding energies, band gaps and band edge positions of C_6H_5CN and $C_6H_5CH_2NH_2$

functionalized MoS₂ at 4%, 6.25%, 11.1%, 12.5%, 18.75% and 25% coverage. The binding energy of ligand to MoS₂ decreases as the increase of the ligand coverage (Fig. 5(a)), which stems from the reduced cross sectional area between the ligand and the surface due to the standing-up of the ligand on the surface with the coverage increase. The band gap of MoS₂ is insensitive to the ligand coverage (see Fig. 5(b)). However, the band edges up-shift gradually with the increase of the ligand coverage, and an abrupt shift is seen when the coverage reaches 18.75% and 25%. This is because the ligand prefers lying on the surface and the perpendicular component of the intrinsic dipole ($\mu_{\text{ligand},\perp}$) is very small when the coverage is less than 12.5%. As the coverage further increases, the ligand begins to lean on MoS₂ with different tilt angles. As a result, $\mu_{\text{ligand},\perp}$ increases obviously, leading to a significant band shift (see Fig. 5(c)). Comparing to C₆H₅CH₂NH₂, the more pronounced band edge shifts brought by C₆H₅CN can be attributed to its larger intrinsic dipole moment (4.702 D vs. 1.407 D).

It is worth pointing out that practical PEC reactions are very complicated and many relevant kinetic processes are still elusive. In fact, the surface functionalization approach only focuses on the thermodynamics, i.e. the energy level alignments. The discussion of kinetic processes is out of the scope of this approach. However, we still think about it. If the surface atoms of MoS₂ serve as reaction sites, the molecular layer will not be beneficial to the reactions, and decrease the available sites. Nevertheless, if MoS₂ only serves as a light adsorber, catalysts can be placed on top of the molecular layer. Or, more practically, if molecular catalysts are adopted, they can be co-adsorbed with the polar molecules on the semiconductor surfaces. Thus, there will be reaction sites above the molecular layer.

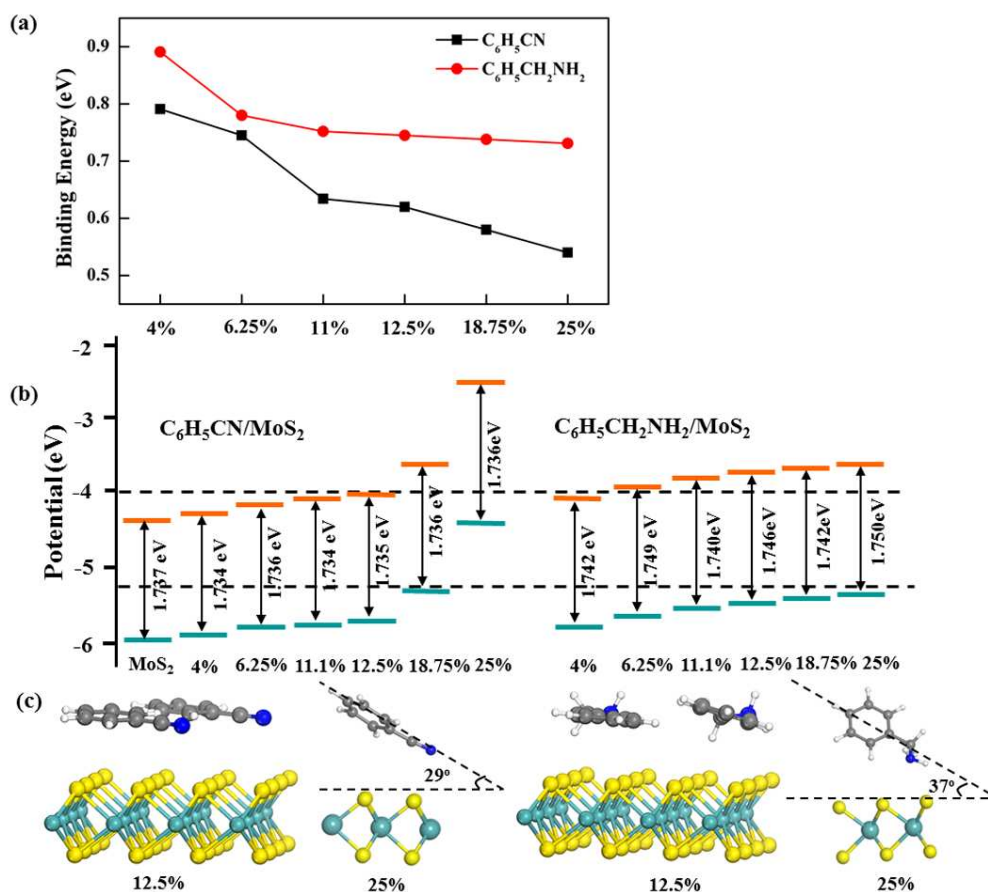


Fig. 5 (a) Binding energies, (b) band gaps and band edge positions of C_6H_5CN and $C_6H_5CH_2NH_2$ functionalized ML-MoS₂, and (c) structure of C_6H_5CN and $C_6H_5CH_2NH_2$ functionalized ML-MoS₂ at 12.5% and 25% coverage.

3.4 Ligand functionalized MoS₂ on graphene substrate

Though ML-MoS₂ exhibits excellent electronic and optical performance, unprotected ML-MoS₂ nanostructures are chemically unstable under practical conditions, leading to many unpredictable results in experiment.^{8,42} Herein, we should add the substrate to protect ML-MoS₂. In practice, graphene is considered as one of the most ideal substrates and hybrid MoS₂/graphene (MoS₂/G) nanostructures have been successfully synthesized experimentally and shown excellent properties⁴³⁻⁴⁷, such as effectively suppressed charge recombination, improved interfacial charge transfer and increased number of active adsorption sites and photocatalytic reaction centers.^{46,47} Here, we use a single layer graphene as the substrate to

protect ML-MoS₂ and investigate the possibility for PEC water-splitting.

Fig. 6(a) shows the fully optimized geometric structure of MoS₂/G, the constituent MoS₂ and graphene retain their respective pristine structural properties. The distance between the two layers is as large as $\sim 3.4 \text{ \AA}$, indicating a very weak coupling between MoS₂ and graphene, which are bound together via vdW interaction. This can also be evidenced by the band structure of MoS₂/G as shown in Fig. 6(b). The band structure of MoS₂ is very similar to that of isolated ML-MoS₂, and graphene preserves its pristine character with linear dispersion bands near the Fermi level. More importantly, due to the existence of interaction between MoS₂ and graphene, the Dirac cone of graphene is opened, forming a tiny band gap of about 2 meV, consistent with the previous study.⁴⁶ Such a small band gap implies the hybrid MoS₂/G nanostructure possesses high carrier mobility, which may be comparable to the free-standing graphene.

Fig. 6(c) displays the band edge positions of the hybrid MoS₂/G together with the water redox potentials. Compared to free-standing MoS₂, the band edges of MoS₂/G changes very little and up-shift by about $\sim 0.06 \text{ eV}$. The shift is because the substrate of graphene breaks the symmetry of MoS₂ and induces the dipole moment. However, the CBM of the MoS₂/G is still below the hydrogen reduction potential, which does not meet the requirement of PEC water-splitting.

We then consider the functionalized MoS₂/G heterostructures with C₆H₅CN and C₆H₅CH₂NH₂ with 12.5% coverage, *e.g.*, hybrid C₆H₅CN/MoS₂/G and C₆H₅CH₂NH₂/MoS₂/G triple-layer nanostructures. The binding energies of ligands to MoS₂/G are 0.682 and 0.796 eV, respectively, larger than the values obtained previously without graphene substrate (0.632 eV

for C_6H_5CN/MoS_2 and 0.745 for $C_6H_5CH_2NH_2/MoS_2$). This indicates that the presence of graphene substrate enhances the stability of ligand functionalized MoS_2 nanostructures. (The binding energy is defined as $E_b = E_{ligand} + E_{MoS_2/G} - E_{ligand/MoS_2/G}$, where E_{ligand} , $E_{MoS_2/G}$ and $E_{ligand/MoS_2/G}$ are energies of isolate ligand, MoS_2/G and ligand/ MoS_2/G). As shown in Fig. 6(b), the band structure of ligand functionalized MoS_2/G is very similar to that of ligand directly functionalized MoS_2 , and the opened band gap of 2 meV is also present. Very interestingly, with the covering of ligands (12.5%), the band edges of ligand functionalized MoS_2/G is tuned to straddle the water redox potential (see Fig. 6(c)). The shifts originate from three aspects including the dipole of MoS_2 induced by the formation of MoS_2 -graphene interface, the intrinsic dipole of the ligand and the induced dipole at ligand/ MoS_2 interface.

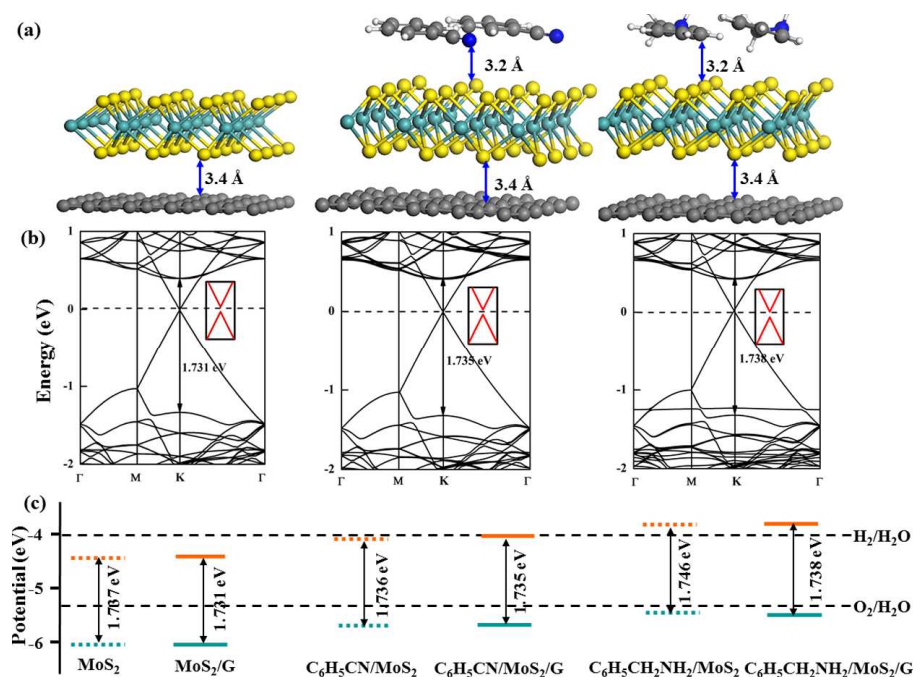


Fig. 6 (a) Optimized structure and (b) band structure of the hybrid MoS_2/G , C_6H_5CN and $C_6H_5CH_2NH_2$ functionalized MoS_2/G at 12.5% ligand coverage, (c) the band edges positions of the MoS_2/G and ligand functionalized MoS_2/G (solid line) at 12.5% ligand coverage in comparison with ligand functionalized MoS_2 (dash line).

4. Conclusion

In summary, based on first-principles electronic structure calculations and analysis of band edge alignment, we have demonstrated that functionalized ML-MoS₂ with ligand is an effective strategy for engineering the band gap and band edges of MoS₂ to meet the requirements of PEC hydrogen production through water-splitting. We found that the ligand functionalization slightly influences the band gap of MoS₂ but greatly affects its band edge positions. The shifts are mainly originated from the intrinsic ligand dipole and the induced dipole at ligand/MoS₂ interface. Furthermore, we can tune the shifts in a large magnitude by choosing suitable ligand groups, functionalizing ligands, controlling ligand coverage and introducing substrate for MoS₂. Our calculations show that C₆H₅CH₂NH₂/MoS₂/G are the strong candidates for PEC water-splitting because of their ideal band gap for optical absorption in visible-light region, high carrier mobility, suitable band edges positions and stable structure for PEC water-splitting. These interesting findings are of fundamental intriguing in their own right, and may also stimulate the experiments to synthesize new functionalized materials for better PEC water splitting.

ACKNOWLEDGMENT

This work is supported by the NBRP (2011CB302004), NSF (11104239, 21373045, 21173040, 1140405) and the NSF of Jiangsu (BK20130016, BK2012322) of China. The authors thank the computational resource at SEU and National Supercomputing Center in Tianjin.

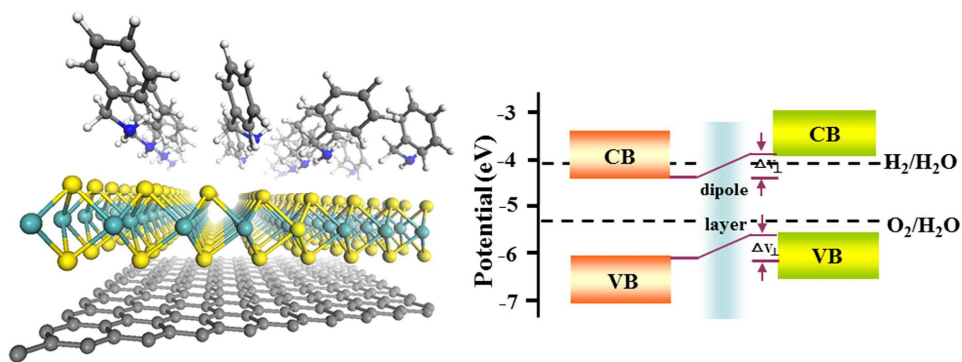
References

- 1 M. Grazel, *Nature*, 2001, **414**, 338.
- 2 A. Kubacka, M. Fernandez-Garcia and G. Colon, *Chem. Rev.*, 2012, **112**, 1555.

- 3 M. R. Hoffmann, S. T. Martin, W. Choi and D. W. Bahnemann, *Chem. Rev.*, 1995, **95**, 69.
- 4 R. Asahi, T. Morikawa, T. Ohwaki, K. Aoki and Y. Taga, *Science*, 2001, **293**, 269.
- 5 A. Fujishima and K. Honda, *Nature*, 1972, **238**, 37.
- 6 W. J. Yin, H. Tang, S. H. Wei, M. M. Al-Jassim, J. Turner and Y. Yan, *Phys. Rev. B*, 2010, **82**, 045106.
- 7 J. Kibsgaard, Z. Chen, B. N. Reinecke and T. F. Jaramillo, *Nat. Mater.*, 2012, **11**, 963.
- 8 B. Radisavljevic, A. Radenovic, J. Brivio, V. Giacometti and A. Kis, *Nat. Nanotech.*, 2011, **6**, 147.
- 9 Y. Li, Z. Zhou, S. B. Zhang and Z. F. Chen, *J. Am. Chem. Soc.*, 2008, **130**, 16739.
- 10 H. Zeng, J. Dai, W. Yao, D. Xiao and X. Cui, *Nat. Nanotech.*, 2012, **7**, 490.
- 11 K. F. Mak, K. He, J. Shan and T. F. Heinz, *Nat. Nanotech.*, 2012, **7**, 494.
- 12 D. Lembke and A. Kis, *ACS Nano.*, 2012, **6**, 10070.
- 13 S. Helveg, J. V. Lauritsen, E. Lægsgaard, I. Stensgaard, J. K. Nøskov, B. S. Clausen, H. Topsøe and F. Besenbacher, *Phys. Rev. Lett.*, 2000, **84**, 951.
- 14 J. V. Lauritsen, J. Kibsgaard, S. Helveg, H. Topsøe, B. S. Clausen, E. Lægsgaard and F. Besenbacher, *Nat. Nanotech.*, 2007, **2**, 53.
- 15 K. K. Kam and B. A. Parkinson, *J. Phys. Chem.*, 1982, **86**, 463.
- 16 K. F. Mak, C. Lee, J. Hone, J. Shan and T. F. Heinz, *Phys. Rev. Lett.*, 2010, **105**, 136805.
- 17 A. Splendiani, L. Sun, Y. Zhang, T. Li, J. Kim, C. Chim, G. Galli and F. Wang, *Nano Lett.*, 2010, **10**, 1271.
- 18 H. Qiu, L. Pan, Z. Yao, J. Li, Y. Shi and X. Wang, *Appl. Lett. Phys.*, 2012, **100**, 123104.
- 19 H. Qiu, T. Xu, Z. Wang, W. Ren, H. Nan, Z. Ni, Q. Chen, S. Yuan, F. Miao, F. Song, G. Long, Y. Shi, L. Sun, J. Wang and X. Wang, *Nat. Commun.*, 2013, **4**, 2642.
- 20 T. F. Jaramillo, K. P. Jørgensen, J. Bonde, J. H. Nielsen, S. Horch and I. Chorkendorff, *Science*, 2007, **317**, 100.
- 21 B. Hinnemann, P. G. Moses, J. Bonde, K. P. Jørgensen, J. H. Nielsen, S. Horch, I. Chorkendorff and J. K. Nørgensen, *J. Am. Chem. Soc.*, 2005, **127**, 5308.
- 22 H. I. Karunadasa, E. Montalvo, Y. Sun, M. Majda, J. R. Long and C. J. Chang, *Science*, 2012, **335**, 698.
- 23 T. R. Thurston and J. P. Wilcoxon, *J. Phys. Chem. B*, 1999, **103**, 11.
- 24 Y. Liu, Y. Yu and W. Zhang, *J. Phys. Chem. C*, 2013, **117**, 12949.
- 25 C. B. Murray, D. J. Norris and M. G. Bawendi, *J. Am. Chem. Soc.*, 1993, **115** (19), 8706.
- 26 W. Wang, S. Banerjee, S. Jia, M. L. Steigerwald and I. P. Herman, *Chem. Mater.*, 2007, **19** (10), 2573.
- 27 S. Yang, D. Prendergast and J. B. Neaton, *Nano Lett.*, 2012, **12**, 383
- 28 B. P. Bloom, L. B. Zhao, Y. Wang and D. H. Waldeck, *J. Phys. Chem. C*, 2013, **117**, 22401.
- 29 M. Yu, P. Doak, I. Tamblyn and J. B. Neaton, *J. Phys. Chem. Lett.*, 2013, **4**, 1701.
- 30 J. P. Perdew, K. Burke and M. Ernzerhof, *Phys. Rev. Lett.*, 1996, **77** (18), 3865.
- 31 S. Grimme, *J. Comput. Chem.*, 2006, **27**, 1787.
- 32 G. Kresse and J. Furthmüller, *Phys. Rev. B.*, 1996, **54**, 11169.
- 33 P. E. Blöchl, *Phys. Rev. B.*, 1994, **50**, 17953.
- 34 J. Neugebauer, M. Scheffler, *Phys. Rev. B.*, 1992, **46**, 16067.
- 35 L. Bengtsson, *Phys. Rev. B.*, 1999, **59**, 12301.
- 36 P. C. Rusu and G. Brocks, *J. Phys. Chem. B*, 2006, **110**, 22628.

- 37 C. Ataca, H. Sahin, E. Akturk and S. Ciraci, *J. Phys. Chem. C*, 2011, **115**, 3934.
- 38 See supporting information at www.rsc.org/nanoscale for further results.
- 39 P. G. Moses, J. J. Mortensen, B. I. Lundqvist and J. K. Nørskov, *J. Chem. Phys.*, 2009, **130**, 104709.
- 40 D. Neamen, *Semiconductor Physics and Devices Basic Principle* (Publishing House of Electronics Industry of China, 4th Ed. 2011).
- 41 W. Tang, E. Sanville and G. Henkelman, *J. Phys.:Condens. Matter*, 2009, **21**, 084204.
- 42 K. S. Novoselov, D. Jiang, F. Schedin, T. J. Booth, V. V. Khotkevich, S. V. Morozov and A. K. Geim, *Proc. Natl. Acad. Sci.*, 2005, **102**, 10451.
- 43 Y. Li, H. Wang, L. Xie, Y. Liang, G. Hong and H. Dai, *J. Am. Chem. Soc.*, 2011, **133**, 7296.
- 44 J. N. Coleman, M. Lotya, A. O'Neill, S. D. Bergin, P. J. King, U. Khan, K. Young, A. Gaucher, S. De, R. J. Smith, I. V. Shvets, S. K. Arora, G. Stanton, H. Kim, K. Lee, G. T. Kim, G. S. Duesberg, T. Hallam, J. J. Boland, J. J. Wang, J. F. Donegan, J. C. Grunlan, G. Moriarty, A. Shmeliov, R. J. Nicholls, J. M. Perkins, E. M. Grieveson, K. Theuwissen, D. W. McComb, P. D. Nellist and V. Nicolosi, *Science*, 2011, **331**, 568.
- 45 S. Min and G. Lu, *J. Phys. Chem. C*, 2012, **116**, 25415.
- 46 Y. Ma, Y. Dai, M. Guo, C. Niu and B. Huang, *Nanoscale*, 2011, **3**, 3883.
- 47 Q. Xiang, J. Yu and M. Jaroniec, *J. Am. Chem. Soc.*, 2012, **134**, 6575.

TOC



Novelty of the work:

This work proposes surface ligand functionalization to tune band edges of monolayer MoS₂ for photoelectrochemical hydrogen production through water-splitting.